

Synthesis and characterization of multifunctional CdTe/Fe₂O₃@SiO₂ core/shell nanosensors for Hg²⁺ ions detection†

Hengguo Wang,^a Yapeng Li,^a Xiaoliang Fei,^a Lei Sun,^a Ligong Zhang,^b Zhenzhong Zhang,^b Yue Zhang,^a Yaoxian Li^a and Qingbiao Yang^{*a}

Received (in Montpellier, France) 25th May 2010, Accepted 26th July 2010

DOI: 10.1039/c0nj00393j

Novel multifunctional magnetic-photoluminescent Hg²⁺ ion sensing nanocomposites were developed by applying SiO₂ as the encapsulation agent to package Fe₂O₃ NRs and CdTe QDs, resulting in CdTe/Fe₂O₃@SiO₂ core/shell nanostructures. The core/shell structural nanocomposites were confirmed by field-emission scanning electron microscopy (FESEM), energy dispersive X-ray analysis (EDXA), X-ray diffraction (XRD) patterns, high-resolution transmission electron microscopy (HRTEM) and selective-area electron diffraction (SAED) patterns. Photoluminescence (PL) spectroscopy and superconducting quantum interference device (SQUID) were used to investigate the optical and magnetic properties of the core/shell structural nanocomposites, respectively. The fluorescence of the obtained nanocomposites could be quenched effectively by Hg²⁺ ions without obvious changes of spectral widths and optical shift of PL emission. The quenching mechanism was studied and the results showed the existence of both static and dynamic quenching processes. The modified Stern–Volmer equation showed a linear response in the range of 1 to 10 μM with a quenching constant (K_{sv}) of $3.5 \times 10^4 \text{ M}^{-1}$. This hydrophilic, biocompatible, multifunctional, easy to separate and sensitive fluorescence nanosensor may find applications in Hg²⁺ ion determination in the biological and environmental areas.

Introduction

Pollution by Hg²⁺ ions around the globe is considered highly dangerous to human health and the environment. Both elemental mercury and ionic mercury can be converted into methyl mercury by bacteria in the environment, which subsequently bioaccumulates through the food chain.¹ Therefore, there is an urgent need to design and develop fluorescent chemosensors that can selectively recognize and determine trace amounts of Hg²⁺ ions, both in environmental analysis and in industrial waste treatment. To date, a variety of fluorescent Hg²⁺ ion chemosensors based on small molecules² and conjugated polymers³ have been reported. However, these chemosensors have some inevitable problems, such as most of them exhibit poor water solubility and suffer photobleaching. So current efforts in this field have focused on the development of water-soluble, photo-stable and separable Hg²⁺ ion sensors.

Semiconductor nanocrystals, often referred to as quantum dots (QDs), have been attracting wide interest due to their excellent optical properties and biological applications.⁴ Indeed, their great water-solubility, wide absorption spectrum, large extinction coefficients, high photoluminescence efficiency,

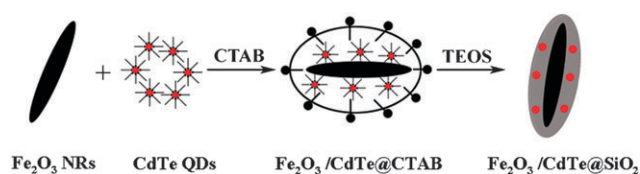
size-dependent emission wavelengths, and sharp emission profile are some of the most attractive characteristics. Furthermore, photobleaching threshold, photostability and chemical stability of QDs are much higher than organic molecules.⁵ Therefore, by virtue of the excellent photophysical properties of QDs, researchers have made efforts toward the development of QD-based fluorescent sensors for detecting metal ions and lots of outstanding improvements have been achieved.⁶ However, in practical applications, separation and recovery of QDs is difficult to control and deal with, remaining an issue to be solved in the field of sensor and biotechnological applications.

Magnetic nanomaterials have also attracted a lot of interest recently because of their excellent function and applications. The excellent separability of the magnetic nanomaterials has been applied extensively in a variety of fields, especially in biotechnology.⁷ Among the magnetic materials, magnetic iron oxide is preferred because it is nontoxic. Consequently, if magnetic Fe₂O₃ nanomaterials are prepared and then combined with QDs, the resulting nanostructures will exhibit both magnetic and fluorescent properties, which should be separable, tunable emission and multifunctional nanocomposite sensors. Building from the above ideas, it is necessary to select an encapsulation agent to integrate these different functionalities. Known for its excellent properties of great hydrophilicity and biocompatibility, intense anti-photobleaching and easy to separate, silica is widely applied as the encapsulation agent to prepare various composite nanostructures. Recently, considerable attention has been focused on the fabrication of composite nanostructures using the performed nanocrystals as building blocks because it can integrate several different functionalities required by the applications into one common nanostructure.⁸

^a Department of Chemistry, Jilin University, Changchun, 130021, People's Republic of China. E-mail: yangqb@jlu.edu.cn; Fax: +86-431-88499576; Tel: +86-431-88499576

^b Key Laboratory of Excited State Processes, Changchun Institute of Optics, Fine Mechanics and Physics, Chinese Academy of Sciences, Changchun, 130033, P. R. China

† Electronic supplementary information (ESI) available: PL spectra of CdTe QDs and CdTe/Fe₂O₃@SiO₂ nanosensors, XPS spectra of nanosensors, fluorescence response of nanosensors upon different metal cations with different concentrations. See DOI: 10.1039/c0nj00393j



Scheme 1 Schematic illustration for preparation of CdTe/Fe₂O₃@SiO₂ core/shell nanostructures.

Herein, we fabricated and characterized the water-soluble, mesoporous CdTe/Fe₂O₃@SiO₂ core/shell nanostructures with magnetic-photoluminescent Hg²⁺ ion-sensing multifunction. We first prepared magnetic Fe₂O₃ nanorods (NRs) and CdTe QDs capped with L-cysteine (L-Cys), and then applied SiO₂ as the encapsulation agent to package Fe₂O₃ NRs and CdTe QDs, giving rise to a novel fluorescent sensor for the determination of Hg²⁺ ions (Scheme 1). The resulting mesoporous SiO₂ shell of the nanocomposites not only seals CdTe QDs inside the nanocomposites but also allows small molecules and ions to enter and contact with the QDs to cause a fluorescence response. The obtained nanosensor was sensitive to the existence of Hg²⁺ ions. Thus a hydrophilic, biocompatible, multifunctional and easy to separate nanosensor for Hg²⁺ ion determination was proposed.

Experimental

Materials

Ferric chloride anhydrous, sodium hydroxide, cadmium chloride, tellurium powders (99.99%), cetyltrimethylammonium bromide (CTAB), tetraethyl orthosilicate (TEOS), ammonium hydroxide and ethanol are all analytical grade (Shanghai Chemical Reagents Co.) and used without further purification. Sodium borohydride (NaBH₄), and L-cysteine (L-Cys) were purchased from Alfa Aesar. The water used in our present work was deionized.

Synthesis of magnetic Fe₂O₃ nanorods (NRs)

Fe₂O₃ NRs were synthesized according to the literature method.⁹ In a typical procedure, 40 mL of 0.5 M FeCl₃ solution was transferred into a 50 mL Teflon-lined autoclave. The autoclave was heated to 120 °C and kept for 12 h. After cooling to room temperature, the resulting precipitates were washed repetitively with deionized water and absolute ethanol, and then dried at 80 °C under vacuum. The as-collected products were calcined at 500 °C for 2.5 h.

Synthesis of L-Cys-stabilized CdTe QDs

L-Cys-Stabilized CdTe QDs were synthesized by reaction of NaHTe and CdCl₂·2.5H₂O following the reported procedures.¹⁰ NaHTe was prepared by the reaction of NaBH₄ and Te powder.¹¹ Typically, a total of 0.2284g CdCl₂·2.5H₂O and 0.2908g of L-Cys were dissolved in 300 mL deionized, and the pH value of the solution was adjusted with NaOH solution (1 M) to 9.0. Then the freshly prepared NaHTe solution was rapidly injected into the reaction mixture. The solution was refluxed at different times and the reaction was terminated to obtain size-controllable QDs with the desired emitting

colors. Adding the isopropanol into the as-prepared solution, the resulting precipitate was centrifuged, washed and dried in a desiccator before use.

Synthesis of mesoporous CdTe/Fe₂O₃@SiO₂ core/shell nanorods

Typically, CdTe QDs (0.08 g), Fe₂O₃ NRs (0.035 g), and CTAB (0.1 g) were dispersed ultrasonically in deionized water (10 mL). Then the as-prepared solution was added to a 100 mL mono-necked round-bottomed flask containing 50 mL of ethanol and 1 mL of water under vigorous stirring. Subsequently, 1.7 mL of ammonium hydroxide (NH₄OH) and 200 μL of TEOS were introduced into the reaction and kept stirring for 12 h at 40 °C. The resulting ternary nanocomposites were obtained by centrifuging and washing with hot water.

Procedures for detection of Hg²⁺ ions

A series of Hg²⁺ ions solutions with different concentrations and 1 mM various metal ions were obtained. 0.05g of CdTe/Fe₂O₃@SiO₂ nanocomposites was dispersed in 20 mL absolute alcohol to form a stable colloidal solution. Then 0.5 mL CdTe/Fe₂O₃@SiO₂ dispersion was injected in the 10 mL Hg²⁺ ions solutions or other various metal ions. Then the fluorescence intensity of the above solution was recorded at about 613 nm with the excitation wavelength of 370 nm.

Characterization

The nanocomposites were characterized by field-emission scanning electron microscopy (FESEM; FEI XL30), energy dispersive X-ray analysis (EDXA, FEI XL30), high-resolution transmission electron microscopy (HRTEM; Hitachi S-570), selective-area electron diffraction (SAED) patterns and X-ray diffraction (XRD; DXP-18AHF diffractometer with Cu-Kα radiation). Magnetization characteristics of the CdTe/Fe₂O₃@SiO₂ nanocomposites were measured with a Quantum Design MPMS-XL SQUID magnetometer. The photoluminescent emission spectra were recorded at room temperature with a Hitachi F-4500 spectrophotometer equipped with a continuous 150 W Xe-arc lamp. X-Ray photoelectron spectroscopy (XPS) was performed using a VG-Scientific ESCALAB 250 spectrometer with a monochromatic Al Kα X-ray source at 1486.6 eV.

Results and discussion

A facile route for the preparation of α-Fe₂O₃ NRs without any templates *via* a hydrothermal process at 120 °C has been used.⁹ The structure and morphology of the initial Fe₂O₃ NRs for preparing the core/shell nanocomposites were investigated by FESEM. As shown in Fig. 1a and b, it can be clearly seen that they are of rod-like morphology with average diameter of about 70–100 nm and a length of about 400–700 nm. And it is interestingly found that the Fe₂O₃ NRs possess a pore structure. After being encapsulated by SiO₂, the resulting CdTe/Fe₂O₃@SiO₂ core/shell nanostructures still maintain the rod-like 1-D morphology with average diameter of about 83–130 nm and a length of about 500–800 nm, as is shown in Fig. 1c. Compared with the pore structure of the as-prepared Fe₂O₃ NRs, the CdTe/Fe₂O₃@SiO₂ core/shell NRs possess a smooth surface. The changes of the surface before and after

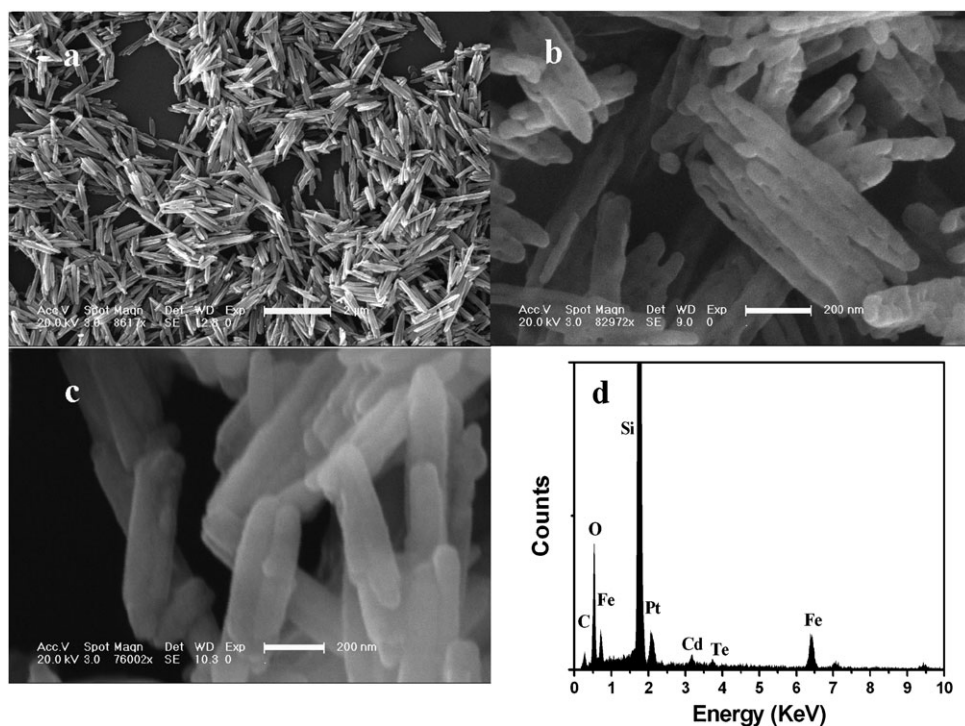


Fig. 1 FESEM images of (a) low and (b) high magnification Fe_2O_3 nanorods; FESEM image (c) of $\text{CdTe}/\text{Fe}_2\text{O}_3@/\text{SiO}_2$ core/shell nanostructures and corresponding EDXA spectrum (d).

SiO_2 coating thus provides experimental proof that the Fe_2O_3 NRs were successfully encapsulated in core/shell nanostructures. The energy dispersive X-ray analysis (EDXA) spectrum shown in Fig. 1d reveals that the core-shell structures consist of C, O, Fe, Si, Cd, and Te elements, which indicated the existence of Fe_2O_3 NRs and CdTe QDs in the nanocomposites. The Pt peaks in the spectrum come from Pt deposited on the tested sample before the measurement and the part of Si comes from the silicon substrates.

The crystal structures of the samples were identified by means of XRD analysis, as shown in Fig. 2. For a comparison, the XRD pattern of the initial Fe_2O_3 NRs is also shown (Fig. 2B). All the diffraction peaks of the product (Fig. 2B) were in agreement with the standard data of $\alpha\text{-Fe}_2\text{O}_3$ (JCPDS No. 33-0664). When the $\alpha\text{-Fe}_2\text{O}_3$ NRs were encapsulated in nanocomposites, the new broad peak located at 2θ values of 23° appeared (Fig. 2A), which is typically caused by amorphous silica. The result indicated that the $\alpha\text{-Fe}_2\text{O}_3$ NRs were successfully encapsulated in SiO_2 . However, it was difficult to detect the reflections corresponding to CdTe QDs, which may be attributed to the low content of CdTe QDs in the nanocomposites and the emerging of the wide peak by the amorphous silica.¹²

Further information about the $\text{CdTe}/\text{Fe}_2\text{O}_3@/\text{SiO}_2$ core/shell nanostructures was obtained from transmission electron microscopy (TEM) images (Fig. 3). From Fig. 3a, it can be seen that the resulting $\text{CdTe}/\text{Fe}_2\text{O}_3@/\text{SiO}_2$ core/shell nanostructures possess the rod-like 1-D morphology with average diameter of about 100 nm and a length of about 500–700 nm, which agrees well with that revealed by the FESEM images. Fig. 3b and c showed the higher magnification TEM and HRTEM images of the $\text{CdTe}/\text{Fe}_2\text{O}_3@/\text{SiO}_2$ core/shell

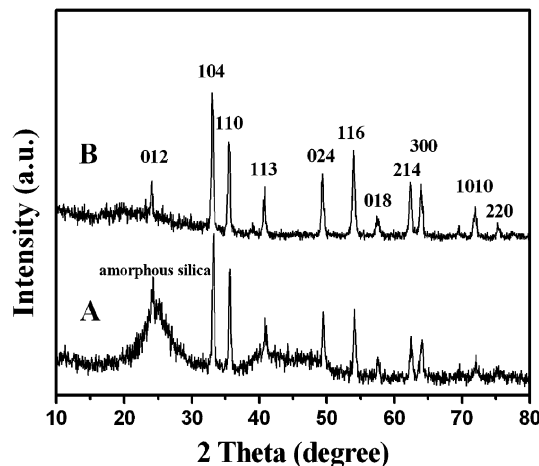


Fig. 2 XRD patterns of (A) $\text{CdTe}/\text{Fe}_2\text{O}_3@/\text{SiO}_2$ core/shell nanostructures and (B) Fe_2O_3 nanorods.

nanostructures, respectively, from which the core/shell structure of the resulting products was clearly observed, also proving that the Fe_2O_3 NRs were embedded within SiO_2 matrix. And we noted that CdTe QDs are mainly adsorbed on the surface of Fe_2O_3 NRs, as indicated by arrows in Fig. 3c. The adsorption of QDs on the surface of Fe_2O_3 NRs, generates therefore a semiconductor-magnetic interface that definitively influences the photoluminescence. As discussed in previous researches,^{8j,k} the embedded Fe_2O_3 NRs significantly reduces the QD fluorescence intensity. This interference of Fe_2O_3 NRs on QD fluorescence is attributed to the iron oxide optical absorption.^{8k} The embedded iron oxide absorbs broadly in the visible spectrum and could thus attenuate both the

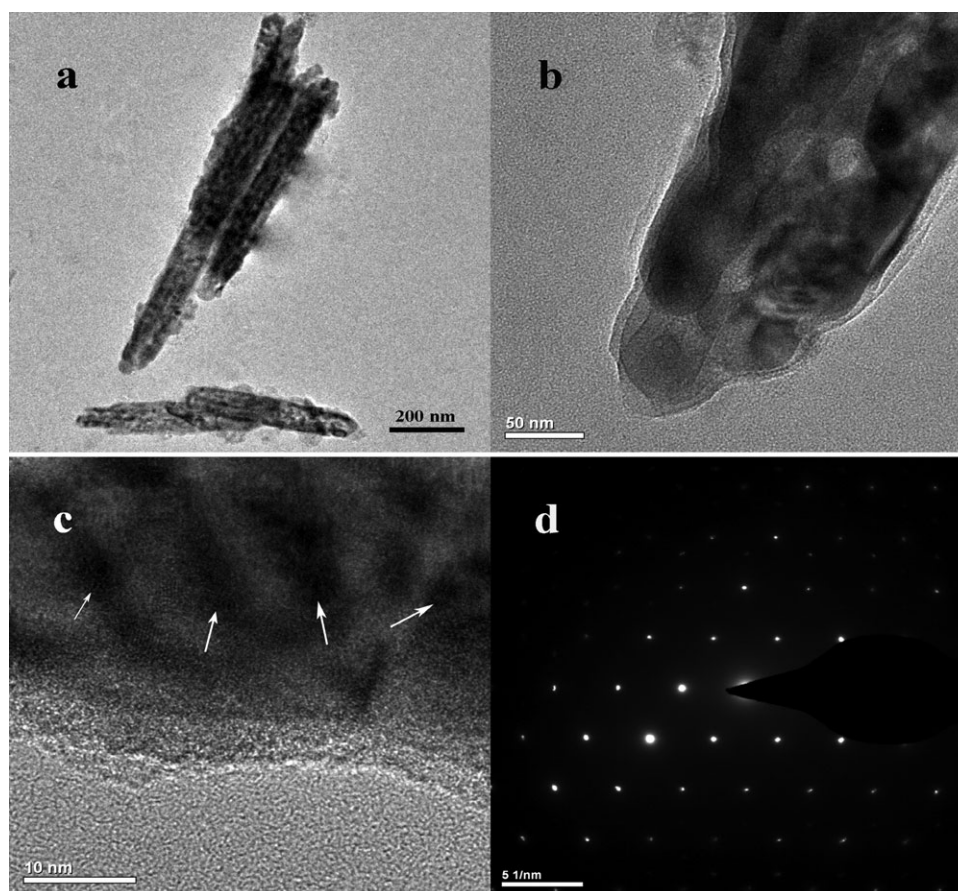


Fig. 3 TEM images of (a) low and (b) high magnification, HRTEM image (c) and SAED pattern (d) of CdTe/Fe₂O₃@SiO₂ core/shell nanostructures.

excitation light and the emitted QD fluorescence. In addition, the normalized PL emission spectra of the QDs and the CdTe/Fe₂O₃@SiO₂ core/shell nanostructures are compared as shown in Fig. S1 (see the ESI†). The maxima of the emission peak are red-shifted (around 6 nm in these cases). The slight red shift in the PL spectrum was observed because the surface state of the QDs was changed by incorporating QDs and Fe₂O₃ NRs into the SiO₂ shell. Obviously, the concentration of TEOS precursor and the hydrolysis time of TEOS had a great effect on the thickness of the shell and the content of CdTe QDs encapsulated.^{8f} To achieve the uniform magnetic seeds with silica coating and strong fluorescence emission from CdTe QDs, we selected the thin silica shell (~4 nm) to combine Fe₂O₃ NRs with QDs. The corresponding selective-area electron diffraction (SAED) patterns were also recorded (Fig. 3d). The regular spots are ascribable to the single-crystallite pattern of α -Fe₂O₃ NRs. The observations above provide further evidence to demonstrate that Fe₂O₃ NRs@SiO₂ core/shell nanostructures are successfully fabricated by the method used in this work.

The magnetic properties of iron oxides have been the focus of extensive research for a long time. The coercivity and magnetic properties carry a direct relationship with the shapes and sizes.¹³ So it is of great significance to investigate the magnetic properties of the CdTe/Fe₂O₃@SiO₂ core/shell nanorods. The magnetic property of the resulting CdTe/Fe₂O₃@SiO₂

core/shell nanostructures was measured by a superconducting quantum interference device (SQUID). Fig. 4 shows the field dependences of magnetization (*M-H* curves) of the nanostructures measured at 300 K. The *M-H* curve displays a strong hysteresis with coercive force of 0.36 T and remnant magnetization of 0.024 emu/g, indicating that the products inherit the strongly ferromagnetic property from the Fe₂O₃ NRs. It is well-known that the magnetization is very sensitive to the structure and morphology (polyhedral, platelike, needlelike, and disk shaped) of particular magnetic materials.¹⁴ Rod-like nanostructures have shape anisotropy in addition to crystalline anisotropy, which is expected to increase the coercivity. Similar phenomena have been observed in porous magnetic α -Fe₂O₃ nanorods, higher coercivity is mainly attributed to higher shape anisotropy and less demagnetizing field because the magnetization is along the long axis.¹⁵

To study the practical applicability, the effect of pH on PL emission intensity of nanosensor was investigated. As shown in Fig. 5, the pH has great effect on the PL emission of CdTe/Fe₂O₃@SiO₂ core/shell nanostructures. One notices that the PL emission intensity of the nanosensor decreased sharply at acidic conditions (pH < 5). With the increase in pH, there was an obvious fluorescence enhancement. So the nanosensor showed the high fluorescence response in neutral and basic pH, which has the same pH profile as that of CdTe QDs itself in aqueous solutions. Considering that most samples

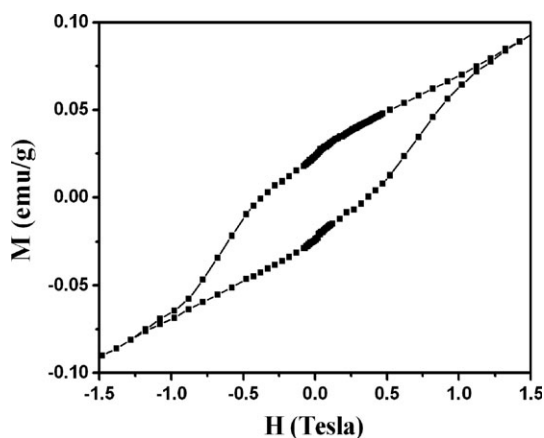


Fig. 4 Magnetic hysteresis loop of the CdTe/Fe₂O₃@SiO₂ core/shell nanostructures measured at 300 K.

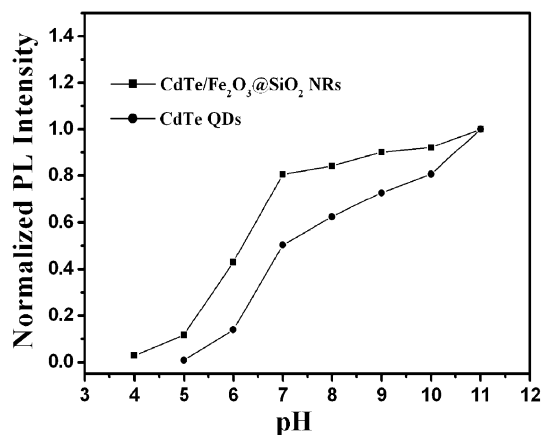


Fig. 5 The influence of pH on the PL emission of CdTe/Fe₂O₃@SiO₂ core/shell nanostructures and CdTe QDs.

for Hg²⁺ ions analysis were neutral, the media for Hg²⁺ ions quantification was then buffered at pH 7.0.

Since herein CdTe/Fe₂O₃@SiO₂ core/shell nanostructures are water-soluble, and the silica shells possess a mesoporous surface, they should be particularly suitable for fluorescent sensor. In order to test the recognition ability of the nanocomposites for Hg²⁺ ions, fluorescence spectra were recorded following excitation at 370 nm at room temperature upon the gradual addition of Hg²⁺ ions into the buffered (pH = 7) solution. Fig. 6 gave detailed fluorescence changes of nanocomposites upon different concentrations of Hg²⁺ ions in the same conditions. When no metal ion was added to the solution of nanocomposites, nanocomposites exhibited very strong fluorescence. Upon the addition of increasing concentrations of Hg²⁺ ions, a significant quenching of the fluorescence of CdTe QDs appeared. Actually, the fluorescence properties of QDs are closely related to the nature of their surfaces.¹⁶ The interactions of QDs with metal ions will cause the modification of the surface of QDs, and as a result, the fluorescence intensity of QDs are quenched.

To determine the sensor mechanism of CdTe/Fe₂O₃@SiO₂ nanocomposites to Hg²⁺ ions, the fluorescence quenching data were analyzed by the Stern–Volmer equation. As is

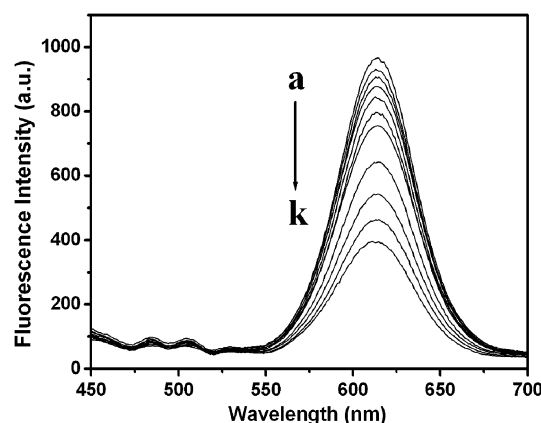


Fig. 6 The PL emission spectra of CdTe/Fe₂O₃@SiO₂ core/shell nanosensor in buffered (NaAc–HAc, pH = 7) solution upon different concentrations of Hg²⁺ ions (0, 0.01, 0.05, 0.1, 0.5, 1, 2, 4, 6, 8 and 10 μM) under excitation of 370 nm.

well-known, the majority of quenching processes can be quantified by the Stern–Volmer equation derived for describing the relationship between excited state quenching and quencher concentration:¹⁷

$$\frac{I_0}{I} = 1 + K_{SV}[Q] \quad (1)$$

where I and I_0 are the luminescence intensities of the CdTe/Fe₂O₃@SiO₂ nanocomposites in the presence and absence of Hg²⁺ ions respectively, $[Q]$ is the Hg²⁺ ions concentration, and K_{SV} is the Stern–Volmer quenching constant. The data obtained by performing a Stern–Volmer analysis in the sensor is shown in Fig. 7. Interestingly, the plots of I_0/I versus Hg²⁺ ions concentration do not fit a conventional linear Stern–Volmer equation. An upward curvature may indicate that both dynamic and static quenching processes occur in this sensor system.^{6j} The dynamic portion of the observed quenching was determined by lifetime measurements using the equation:

$$\frac{\tau_0}{\tau} = 1 + K_D[Q] \quad (2)$$

where τ_0 and τ are the fluorescence lifetimes of CdTe/Fe₂O₃@SiO₂ nanocomposites in the absence and presence of Hg²⁺ ions

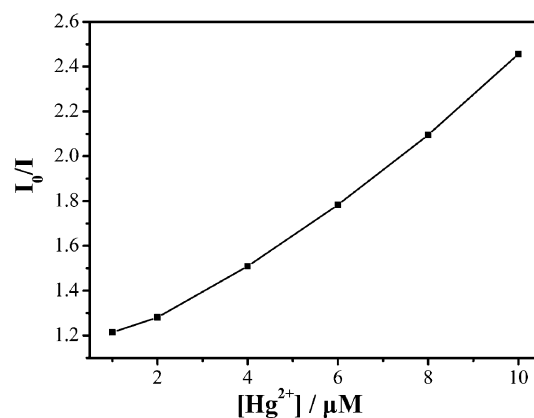


Fig. 7 Stern–Volmer plot for interaction between CdTe/Fe₂O₃@SiO₂ nanosensor and Hg²⁺ ions.

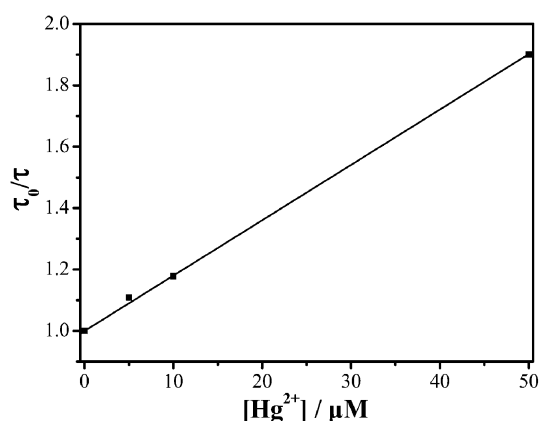


Fig. 8 Stern–Volmer plot of the excited state lifetimes of CdTe/Fe₂O₃@SiO₂ nanosensor in the absence (τ₀) and presence of different Hg²⁺ ions concentrations.

respectively, and K_D is the dynamic quenching constant. The fluorescence lifetime of CdTe/Fe₂O₃@SiO₂ nanocomposites in the presence of different concentrations of Hg²⁺ ions were recorded. From one-exponential law of the fluorescence decay curves, the fluorescence lifetime of QDs decreased from 10.2 ns in the absence of Hg²⁺ ion to 9.2, 8.6, and 5.4 ns in the presence of increasing concentrations of Hg²⁺ ion from 5, 10, to 50 μmol L⁻¹, respectively. The plot of τ₀/τ against the concentration of added Hg²⁺ ion is depicted in Fig. 8, which exhibits a linear relationship. The value of K_D was obtained from this plot and was found to be 1.8×10^4 M⁻¹.

The value of static quenching constant, K_S , was obtained using the equation below:

$$\frac{I_0}{I} = 1 + (K_D + K_S)[Q] + K_D K_S [Q]^2$$

The graph of $(I_0/I - 1)/[Q]$ versus $[Q]$ is plotted using the value of K_D obtained from the lifetime measurements. K_S was found to be 1.1×10^5 M⁻¹. This indicates that the fluorescence of CdTe/Fe₂O₃@SiO₂ nanocomposites is quenched by Hg²⁺ ions through both dynamic and static quenching mechanisms. Considering the greater static quenching constant, the static quenching mechanism is predominantly operative in this system.

Both static and dynamic quenching require molecular contact between the fluorophore and the quencher. In this system, the Hg²⁺ ions diffuse the fluorescence of the CdTe/Fe₂O₃@SiO₂ nanocomposites during the lifetime of the excited state, causing the collisional quenching. Upon contact the CdTe/Fe₂O₃@SiO₂ nanocomposites return to the ground state without emitting a photon. In the case of static quenching, a non-fluorescent ground-state CdTe–Hg²⁺ complex can be formed between the Hg²⁺ ions and the surface ligands of CdTe QDs.⁶⁰ This prediction was verified by the results of XPS analysis (see the ESI†, Fig. S2). The mercury peaks in the XPS spectra demonstrate that Hg²⁺ ions exist in the nanocomposites. This may be attributed to the binding of Hg²⁺ ions onto the QDs surface due to the strong affinity of Hg²⁺ ions with the surface ligands of CdTe QDs. In addition, the complexation of Hg²⁺ ions by surface of the QDs provokes an effective electron transfer process on the

surface of the QDs.^{6b} So a complex quenching mechanism is caused by both ion binding and electron transfer acted together. Considering no maximum FL emission wavelength red shift in the process of quenching, the quenching of FL emission of QDs by Hg²⁺ ions is attributed to ion binding followed by a charge transfer process on the surface of the QDs.

A modified Stern–Volmer relationship which has already been proposed for the systems involving the mechanisms where both static and dynamic quenching of fluorescence of QDs exist was utilized to obtain a calibration plot.^{6b,h,i,k}

$$\text{Log}\left(\frac{I_0}{I}\right) = K_{SV}[Q] + C$$

where I and I_0 are the luminescence intensities of the CdTe/Fe₂O₃@SiO₂ nanocomposites in the presence and absence of Hg²⁺ ions respectively, $[Q]$ is the Hg²⁺ ion concentration, K_{SV} is the Stern–Volmer quenching constant and C is the constant of equation. The equation reveals that I_0/I increase in direct proportion to the concentration of the quencher. As is shown in Fig. 9, a very good linearity between I_0/I and concentration of quencher Hg²⁺ in the range of 1 to 10 μM is obtained with a linearly dependent coefficient R^2 of 0.999. From slopes of the plot, the Stern–Volmer constant (K_{sv}) is calculated to be 3.5×10^4 M⁻¹ for Hg²⁺ ions. This order of magnitude is compatible with the formation of a quite stable complex between the nanosensor and Hg²⁺ ions.

In order to test the practical application of the nanosensor for Hg²⁺ ions, the interference of other metal ions on the PL emission intensity of the CdTe/Fe₂O₃@SiO₂ core/shell nanosensor was also studied. In certain environmental samples, such as river and seawater, the concentrations of some prevalent toxic metal ions are significantly higher, therefore, the higher concentration (1 mM) of K⁺, Na⁺, Ba²⁺, Ca²⁺, Cd²⁺, Pb²⁺, Mg²⁺, Zn²⁺ and Co²⁺ ions, were added to the nanosensor solution, and the PL emission intensity of the nanosensor upon addition of various metal cations was depicted in Fig. 10. As shown in Fig. 10, the above-mentioned

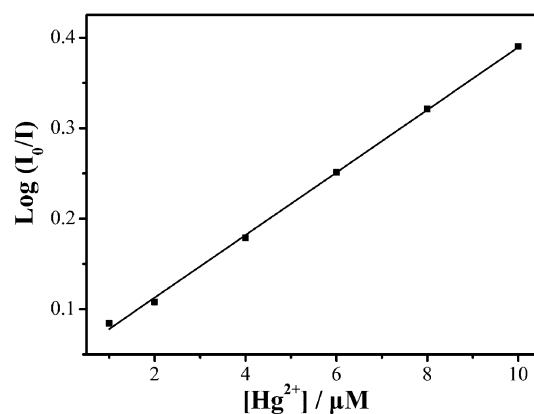


Fig. 9 Modified Stern–Volmer plot of the quenching of the fluorescence of CdTe/Fe₂O₃@SiO₂ core/shell nanosensor versus the concentration of Hg²⁺ ions.

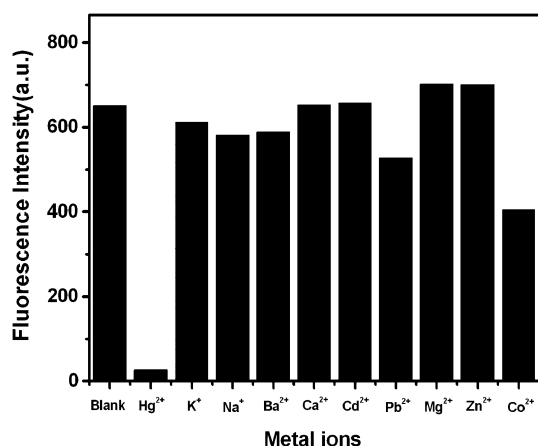


Fig. 10 Fluorescence response of CdTe/Fe₂O₃@SiO₂ core/shell nanosensor in buffered (NaAc–HAc, pH = 7) solution upon various metal cations (1 mM) with an excitation at 370 nm.

metal ions show weak effect on the fluorescence intensity of the nanosensor. However compared with the marked quenching provoked by Hg²⁺ ions, the influence of the above-mentioned metal ions is negligible. Unfortunately, Ag⁺ and Cu²⁺ ions (1 mM) can cause strong quenching of the fluorescence intensity of the nanosensor (see the ESI†, Fig. S3a), therefore, they can be considered as interfering species. But when the concentration of these ions was lowered to 0.01 mM, the quenching effects were weak (see the ESI†, Fig. S3b and 3c). Thus these interferences can be diminished by diluting the sample.⁶¹

Conclusions

In summary, a hydrophilic, biocompatible, multifunctional and easy to separate nanosensor for Hg²⁺ ions determination was developed by applying SiO₂ as the encapsulation agent to package Fe₂O₃ NRs and CdTe QDs, resulting in CdTe/Fe₂O₃@SiO₂ core/shell nanostructures. The core/shell nanocomposites showed high sensitivity for Hg²⁺ ions. The quenching provoked by Hg²⁺ ions is caused by the cooperation of static and dynamic quenching processes. Considering no maximum FL emission wavelength red shift in the process of quenching, the quenching of FL emission of QDs by Hg²⁺ ions is attributed to ion binding followed by a charge transfer process on the surface of QDs. A combination of magnetic, photoluminescent and Hg²⁺ ion-sensing properties make them promising candidates for cell separation, biomarkers and determination of Hg²⁺ ions concentration in environmental and biological systems.

Acknowledgements

The authors gratefully acknowledge the support of the National Natural Science Foundation of China (No. 20874033).

References

- 1 H. G. Seiler, A. Sigel and H. Sigel, *Handbook on Metals in Clinical and Analytical Chemistry*, Marcel Dekker, New York, 1994.

- 2 (a) H. N. Kim, M. H. Lee, H. J. Kim, J. S. Kim and J. Yoon, *Chem. Soc. Rev.*, 2008, **37**, 1465–1472; (b) E. M. Nolan and S. J. Lippard, *Chem. Rev.*, 2008, **108**, 3443–3480; (c) E. M. Nolan and S. J. Lippard, *J. Am. Chem. Soc.*, 2007, **129**, 5910–5918; (d) A. Coskun and E. U. Akkaya, *J. Am. Chem. Soc.*, 2006, **128**, 14474–14475; (e) A. Ono and H. Togashi, *Angew. Chem., Int. Ed.*, 2004, **43**, 4300–4302; (f) D. Wu, A. B. Descalzo, F. Weik, F. Emmerling, Z. Shen, X. Z. You and K. Rurack, *Angew. Chem., Int. Ed.*, 2008, **47**, 193–197.
- 3 (a) S. W. Thomas, G. D. Joly and T. M. Swager, *Chem. Rev.*, 2007, **107**, 1339–1386; (b) L. J. Fan, Y. Zhang and W. E. Jones, *Macromolecules*, 2005, **38**, 2844–2849; (c) X. F. Liu, Y. L. Tang, L. H. Wang, J. Zhang, S. P. Song, C. H. Fan and S. Wang, *Adv. Mater.*, 2007, **19**, 1662.
- 4 (a) A. Jayagopal, Y. R. Su, J. L. Blakemore, M. F. Linton, S. Fazio and F. R. Haselton, *Nanotechnology*, 2009, **20**, 165102; (b) T. Dutta, M. Garg and N. K. Jain, *Eur. J. Pharm. Sci.*, 2008, **34**, 181–189.
- 5 (a) M. Bruchez, M. Jr Moronne, P. Gin, S. Weiss and A. P. Alivisatos, *Science*, 1998, **281**, 2013–2016; (b) W. C. W. Chen and S. Nie, *Science*, 1998, **281**, 2016–2018.
- 6 (a) Y. S. Xia and C. Q. Zhu, *Talanta*, 2008, **75**, 215–221; (b) J. Chen, Y. Gao, Z. Xu, G. Wu, Y. Chen and C. Zhu, *Anal. Chim. Acta*, 2006, **577**, 77–84; (c) M. C. Mancini, B. A. Kairdolf, A. M. Smith and S. Nie, *J. Am. Chem. Soc.*, 2008, **130**, 10836–10837; (d) J. L. Chen and C. Q. Zhu, *Anal. Chim. Acta*, 2005, **546**, 147–153; (e) E. M. Ali, Y. Zheng, H. Yu and J. Y. Ying, *Anal. Chem.*, 2007, **79**, 9452–9458; (f) Y. Chen and Z. Rosenzweig, *Anal. Chem.*, 2002, **74**, 5132–5138; (g) J. G. Liang, X. P. Ai, Z. K. He and D. W. Pang, *Analyst*, 2004, **129**, 619–622; (h) W. J. Jin, J. M. Costa-Fernandez, R. Pereiro and A. Sanz-Medel, *Anal. Chim. Acta*, 2004, **522**, 1–8; (i) Y. Xia and C. Zhu, *Analyst*, 2008, **133**, 928–932; (j) R. J. Herturbise, A. H. Ackerman and B. W. Smith, *Appl. Spectrosc.*, 2001, **55**, 490–495; (k) G. H. Shi, Z. B. Shang, Y. Wang, W. J. Jin and T. C. Zhang, *Spectrochim. Acta, Part A*, 2008, **70**, 247–252; (l) C. Wang, J. W. Zhao, Y. Wang, N. Lou, Q. Ma and X. G. Su, *Sens. Actuators, B*, 2009, **139**, 476–482; (m) A. V. Isarov and J. Chrysochoos, *Langmuir*, 1997, **13**, 3142–3149; (n) C. Dong, H. Qian, N. Fang and J. Ren, *J. Phys. Chem. B*, 2006, **110**, 11069; (o) M. Koneswaran and R. Narayanaswamy, *Sens. Actuators, B*, 2009, **139**, 104–109.
- 7 (a) P. L. Kronick, G. L. Campbell and K. Joseph, *Science*, 1978, **200**, 1074–1076; (b) H. A. Oktem, G. Bayramoglu, V. C. Ozalp and M. Y. Arica, *Biotechnol. Prog.*, 2007, **23**, 146; (c) A. G. Hu, G. T. Yee and W. B. Lin, *J. Am. Chem. Soc.*, 2005, **127**, 12486–12487.
- 8 (a) G. Z. Shen, Y. Bando, C. H. Ye, X. L. Yuan, T. Sekiguchi and D. Golberg, *Angew. Chem., Int. Ed.*, 2006, **45**, 7568; (b) P. Yang, M. Ando and N. Murase, *New J. Chem.*, 2009, **33**, 1457–1461; (c) P. Yang, M. Ando and N. Murase, *New J. Chem.*, 2009, **33**, 561–567; (d) Y. Li, Q. Zhang, A. V. Nurmikko and S. Sun, *Nano Lett.*, 2005, **5**, 1689–1692; (e) T. Pellegrino, A. Fiore, E. Carlino, C. Giannini, P. D. Cozzoli, G. Ciccarella, M. L. Respaud, R. Cingolani and L. Manna, *J. Am. Chem. Soc.*, 2006, **128**, 6690–6698; (f) Y. Song, X. Cao, Y. Guo, P. Chen, Q. Zhao and G. Shen, *Chem. Mater.*, 2009, **21**, 68; (g) S. T. Selvan, P. K. Patra, C. Y. Ang and J. Y. Ying, *Angew. Chem., Int. Ed.*, 2007, **46**, 2448–2452; (h) J. Kim, J. E. Lee, J. Lee, J. H. Yu, B. C. Kim, K. An, Y. Hwang, C. H. Shin, J. G. Park, J. Kim and T. Hyeon, *J. Am. Chem. Soc.*, 2006, **128**, 688–689; (i) H. w. Gu, R. k. Zheng, X. X. Zhang and B. Xu, *J. Am. Chem. Soc.*, 2004, **126**, 5664–5665; (j) D. S. Wang, J. B. He, N. Rosenzweig and Z. Rosenzweig, *Nano Lett.*, 2004, **4**, 409–413; (k) T. R. Sathe, A. Agrawal and S. M. Nie, *Anal. Chem.*, 2006, **78**, 5627–5632.
- 9 Y. J. Chen, C. L. Zhu, X. L. Shi, M. S. Cao and H. B. Jin, *Nanotechnology*, 2008, **19**, 205603.
- 10 Y. Liu, W. Chen, A. G. Joly, Y. Wang, C. Pope, Y. Zhang, J. O. Bovin and P. Sherwood, *J. Phys. Chem. B*, 2006, **110**, 16992–17000.
- 11 D. L. Klayman and T. S. Griffin, *J. Am. Chem. Soc.*, 1973, **95**, 197–199.
- 12 X. B. Cao, X. M. Lan, Y. Guo and C. Zhao, *Cryst. Growth Des.*, 2008, **8**, 575–580.

- 13 (a) C. Gong, D. Chen, X. Jiao and Q. Wang, *J. Mater. Chem.*, 2002, **12**, 1844–7; (b) H. Itoh and T. Sugimoto, *J. Colloid. Interface Sci.*, 2003, **265**, 283–95.
- 14 M. Sorescu, R. A. Brand, D. M. Tarabasanu and L. Diamandescu, *J. Appl. Phys.*, 1999, **85**, 5546–8.
- 15 N. K. Chaudhari and J. S. Yu, *J. Phys. Chem. C*, 2008, **112**, 19957–62.
- 16 (a) U. Woggon, *Optical Properties of Semiconductor Quantum Dots*, Springer, Berlin, Germany, 1997; (b) N. Myung, Y. Bae and A. J. Bard, *Nano Lett.*, 2003, **3**, 747–749; (c) P. Reiss, J. Bleuse and A. Pron, *Nano Lett.*, 2002, **2**, 781–784.
- 17 J. R. Lakowicz, *Principles of Fluorescence Spectroscopy*, Springer, New York, 3rd edn, 2006.